Solar Energy 188 (2019) 1248–1255

Contents lists available at ScienceDirect

Solar Energy

journal homepage: www.elsevier.com/locate/solener

Luminescent solar concentrators performing under different light conditions

Yilin Li[a,b,*], Yujian Sun[a,c], Yongcao Zhang[d]

[a] Solera City Energy, Harbin, Heilongjiang 150000, China
[b] Department of Chemical and Biomolecular Engineering, Rice University, Houston, TX 77005, United States
[c] School of Environmental and Forest Sciences, University of Washington, Seattle, WA 98195, United States
[d] Department of Mechanical Engineering, University of Houston, Houston, TX 77004, United States

ARTICLE INFO

Keywords:
Luminescent solar concentrator
Power conversion efficiency
Power concentration ratio
Outdoor
Indoor
Light condition

ABSTRACT

The use of luminescent solar concentrators (LSCs) is considered a promising option to impart energy harvesting capability to buildings with minimal alternation to the building structure. To fill the gap between fundamental research and practical application, this study investigated the performance (power conversion efficiency, η_{LSC} and power concentration ratio, C) of the LSCs of different sizes under different light conditions including simulated sunlight condition, outdoor sunny, overcast and raining conditions, and indoor condition employing four different types of light bulbs (*i.e.*, incandescent, halogen, fluorescent and light-emitting diode). It was observed that the LSCs exhibited higher one-sun performance under outdoor sunny condition than under simulated sunlight. Under overcast and raining conditions, η_{LSC} decreased significantly with the increase of the device size. Under indoor incandescent and halogen light conditions, the LSCs exhibited low η_{LSC} due to the low percentage of the visible portion in the light spectrum. Surprisingly high η_{LSC} boosted by 50% compared to the outdoor sunny condition was obtained in the LSCs under fluorescent and LED light conditions. This research suggested very promising application of the LSCs in indoor light energy recycling, which has not been proposed before.

1. Introduction

Though the concept of luminescent solar concentrators (LSC) was proposed more than thirty years ago (Weber and Lambe, 1976; Goetzberger and Greube, 1977), it was reintroduced to the research community a decade ago and the relevant research regained its momentum in recent years for the promising application of the LSCs in net-zero-energy buildings and the feasible integration of the LSCs to the built environment (Debije and Verbunt, 2012; van Sark et al., 2008). An LSC consists of an optical waveguide that is doped with luminophores and solar cells attached to the edge of the waveguide (Fig. 1a). In a typical operation under sunlight, short-wavelength photons are collected on the large front surface of the waveguide and converted by the luminophores to long-wavelength photons, which follow successive total internal reflection (TIR) and transport to the edge-attached solar cells (Li et al., 2019). The capability to work optimally under direct and indirect light conditions (Debije and Rajkumar, 2015) and the tunable color or even transparency (Zhao and Lunt, 2013; Zhao et al., 2014; Yang et al., 2018) by the employment of different luminophores allow the LSCs to access the places where conventional solar panels can't, especially working and living areas in the built environment (Reinders et al., 2018). LSCs has demonstrated huge potential to replace conventional glass-based building envelope such as windows, facades and atriums (Kerrouche, 2014; van Sark et al., 2017), and to contribute to the energy efficiency of the buildings that are constructed with photovoltaic structures (Zalewski et al., 2002; Akwa et al., 2014; Lai and Hokoi, 2015; Li and Liu, 2018; Powell et al., 2018; Kang et al., 2019).

There is no doubt that over the past years significant advancement has been made in the research of the LSCs. Numerous efforts have been taken to enhance the device performance through the search for luminophores with ideal spectroscopic properties. Organic dyes (Sanguineti et al., 2013; Mouedden et al., 2015; Li et al., 2016), quantum dots (Purcell-Milton and Gun'ko, 2012; Zhou et al., 2018; Moraitis et al., 2018) and rare-earth complexes (Liu et al., 2014; Freitas et al., 2015; Frias et al., 2019) are three primary categories, in which luminophores are developed with wide absorption range that covers the solar spectrum up to the band gap of the solar cell (Shcherbatyuk et al., 2010; Meinardi et al., 2015; Zhou et al., 2016), red-shifted emission that matches the band gap of the solar cell (Sanguineti et al., 2012; Chen et al., 2017; Yang et al., 2019), minimal spectral overlap that addresses the self-absorption issue (Meinardi et al., 2017; ten Kate et al., 2015; Wang et al., 2011), and near-unity photoluminescence quantum yield

* Corresponding author.
E-mail address: yilinli@rice.edu (Y. Li).

https://doi.org/10.1016/j.solener.2019.07.035
Received 25 May 2019; Received in revised form 6 July 2019; Accepted 9 July 2019
Available online 12 July 2019

(PLQY) that indicates almost no photon number loss during the process of spectroscopic conversion (Knowles et al., 2015; Zhang et al., 2018; Bergren et al., 2018). In addition, various light trapping techniques have been developed to maximize the photon collection or minimize the photon loss of the LSCs. For example, optical lens (Tseng et al., 2011; Tsoi et al., 2013; Damrongsak and Locharoenrat, 2017; Kurmi et al., 2018) and plasmonic effects (Chandra et al., 2012; Tummeltshammer et al., 2013; Fahad et al., 2017) have been implemented to increase the intensity of the incidence. Wavelength-selective mirrors (Debije et al., 2010; Verbunt et al., 2012; Connell et al., 2018) and distributed Bragg reflectors (Xu et al., 2016; Connell and Ferry, 2016; Iasilli et al., 2019) have been employed to reduce the photon escaping cone loss from the waveguide surface.

Compared to the numerous reports on the luminophores and techniques developed for the LSCs, there are handful studies focusing on the performance of the LSCs under different light conditions. Indeed, different light conditions has different impacts on the performance of the LSCs. For example, devices configured in an outdoor environment such as a building envelope (Fig. 1b) would perform differently from those applied in an indoor environment such as an office area (Fig. 1c) because of the difference in light spectrum and intensity. In this report, we present studies on the performance of the LSCs under different light conditions (*e.g.*, standard, non-standard, direct, indirect, outdoor and indoor). This research suggests a new possible direction in application of the LSCs.

2. Methodology

2.1. Materials

All chemicals were used as received without further purification. The renowned BASF Lumogen F Red 305 (R305) was chosen as luminophores in the LSCs (Wilson et al., 2010; Sala et al., 2019; Griffini et al., 2013). The chemical name of R305 is *N*; *N*′-bis(2,6-diisopropylphenyl)-1,6,7,12-tetraphenoxy-3,4,9,10-perylenetetracarboxylic diimide. It was purchased from TCI America. The monomer methyl methacrylate (MMA) and the radical initiator azobisisobutyronitrile (AIBN) was purchased from Sigma-Aldrich. The polycrystalline (p-Si) solar cells were purchased from eBay. Incandescent (GE), halogen (Globe), fluorescent (GE) and light-emitting diode (LED) (EnergySmart) light bulbs were purchased from Amazon.

2.2. Device fabrication

The fabrication of the LSCs was according to the procedure in literature (Fig. 2) (Li et al., 2016). Free radical polymerization was employed to fabricate the luminescent waveguide. Luminophores (60 ppm) and radical initiator (0.1 w/w%) was dissolved in MMA in an Erlenmeyer flask, and the solution was stirred in a water bath at 85 °C. When the viscosity of the solution was higher than that of glycerol, heating was stopped, and the flask was placed into an ice/water bath at 0 °C. After being cooled down, the syrup was poured into a glass mold. The mold was placed in an incubator at 45 °C for 48 h. After the syrup turned into solid, the mold was transferred to an oven and further cured at 100 °C for 2 h. After being cooled down, the raw luminescent waveguide can be easily separated from the glass mold, followed by cutting into square shapes and edge polishing. The thickness of the waveguide was 0.25 in., and the length was from 1 in. to 12 in. The optical density (OD) of the waveguide was 4 with 5% variation. The variation was due to the shrinkage of the raw waveguide volume by 20% during polymerization. The OD of 4 was equivalent to that 99.99% of the incident photons was absorbed at the absorption maximum of the luminophores. The p-Si solar cells were then glued to the four edges of the waveguide using UV-curing optical adhesives. They were connected in parallel to maximize the device performance (Slooff et al., 2008).

2.3. Instrumentation

Absorption spectrum of the luminophores and transmission spectrum of the luminescent waveguide were measured using a Varian Cary 5000 UV–Vis–NIR spectrometer. Emission spectra of the luminophores and the light bulbs were recorded on an ISS PC1 photon counting spectrofluorometer. The PLQYs were measured using an integrating sphere connected to a Hamamatsu C9920-12 external quantum efficiency (EQE) measurement system. An OAI class AAA solar simulator was used to provide simulated AM1.5G sunlight. The *J-V* curves were measured by a Keithley 2401 sourcemeter. The EQE spectrum of the solar cell was performed on an Enlitech QE-R3011 system. The incident power density (P_{in}) of indoor and outdoor conditions was measured by an Amprobe SOLAR-100 solar power meter.

2.4. Light condition

The outdoor light condition included sunny, overcast and raining conditions. The corresponding P_{in} were $1000\,W{\cdot}m^{-2} \pm 100\,W{\cdot}m^{-2}$, $100\,W{\cdot}m^{-2} \pm 10\,W{\cdot}m^{-2}$ and $50\,W{\cdot}m^{-2} \pm 5\,W{\cdot}m^{-2}$, respectively. The measurement was performed between May and September in Seattle, and the local temperature was between 32 °C and 38 °C. In the sunny condition, the device was oriented towards to the solar radiation (Fig. 3a). The elevation angle of the sun was between 50° and 70°. The

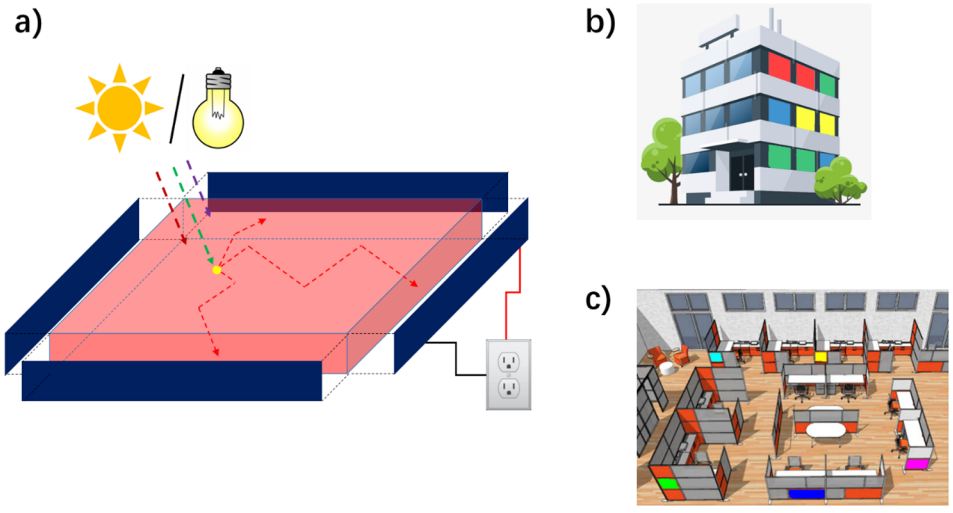

Fig. 1. Schematic representations of (a) the operational mechanism of an LSC, and the application of the LSCs in (b) a building envelope and (c) an office area.

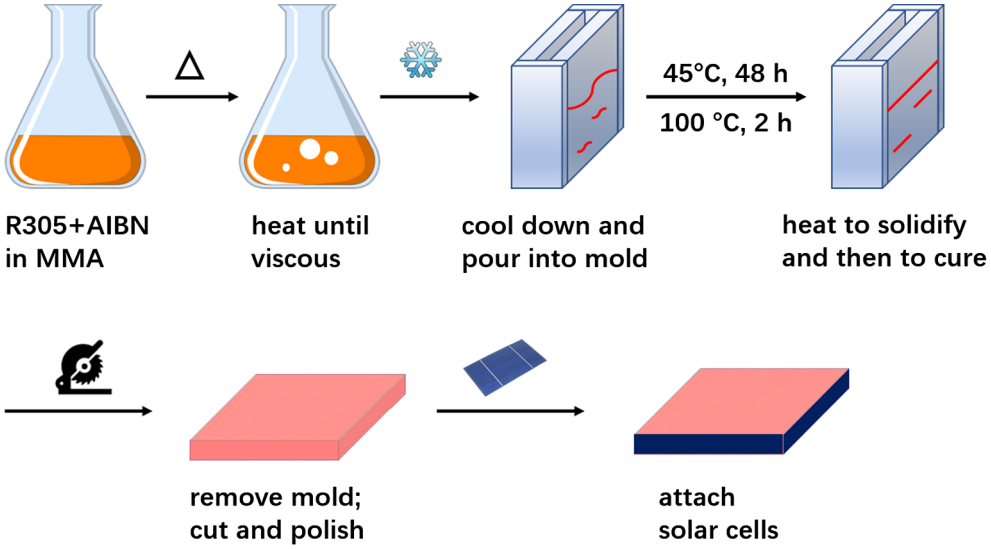

Fig. 2. Fabrication procedure of the LSCs.

indoor light condition was achieved by utilizing an array of light bulbs in a box, which was coated with diffuse reflective layers to obtain an environment of diffuse light (Fig. 3b). A separator that was also coated with diffuse reflective layers was placed between the light bulbs and the device to avoid direct illumination. The brightness of the light bulbs was adjusted to achieve a P_{in} of 10 W·m^{-2} ± 1 W·m^{-2}.

3. Results and discussion

3.1. Properties of the luminophores and solar cells

We first investigated the spectroscopic properties of R305 and photovoltaic properties of p-Si solar cells because the spectroscopic and photovoltaic data obtained in this study were used for the model projection of device performance. The spectroscopic properties of R305 were measured in PMMA matrix, which was a small piece cut from the luminescent waveguide. The absorption spectrum of R305 maximized at 574 nm with a shoulder at 535 nm, indicating a weak intramolecular charge transfer (ICT) electronic transition (Fig. 4a) (Li et al., 2012, 2013). It also possessed a peak in short-wavelength region at 437 nm, ascribing to the π-π* electronic transition (Li et al., 2015). The emission spectrum of R305 centered at 605 nm, resulting in a Stokes shift of 31 nm relative to the absorption maximum. This small Stokes shift apparently led to a large spectral overlap with the self-absorption cross section per 1 cm optical path (σ_{SA}) of 26% (Krumer et al., 2013). The PLQY of R305 was dependent on the excitation wavelength (Fig. 4b). The lowest PLQY was 0.56 at 380 nm and the highest was 0.94 at 540 nm. The average PLQY calculated over the AM1.5G solar spectrum was 0.85. As of the luminescent waveguide, it exhibited a near 0% transmission from 500 nm to 600 nm and a low transmission of 10% to short-wavelength light (Fig. 4c). From the spectral analysis, the waveguide absorbed 28% photons in the solar spectrum before the band gap of p-Si (E_g = 1.1 eV or 1100 nm) (Fig. 4d).

The photovoltaic parameters of the p-Si solar cells were extracted from the *J-V* curve measured under AM1.5G simulated sunlight. The solar cells in average possessed short circuit current density (J_{sc}) of 330 A·m^{-2}, open circuit voltage (V_{oc}) of 0.62 V, and fill factor (*FF*) of 0.76 (Fig. 4e). The corresponding power conversion efficiency of the solar cells (η_{cell}) is 15.5%. The external quantum efficiency (EQE) of the solar cells maximized at 0.86 around 600 nm (Fig. 4f) and matched the emission maximum of R305. The performance of the solar cells under different incident power density (P_{in}) was also studied. The maximum power density of the solar cells (P_{max}) demonstrated a linear increase (Fig. 4g), while the corresponding η_{cell} increased and then reached to a plateau with the increase of P_{in} (Fig. 4h). A relatively low η_{cell} of 13.9% was obtained at a low P_{in} of 100 W·m^{-2}, while η_{cell} kept apparently as a constant of 15.5% when P_{in} was greater than 700 W·m^{-2}.

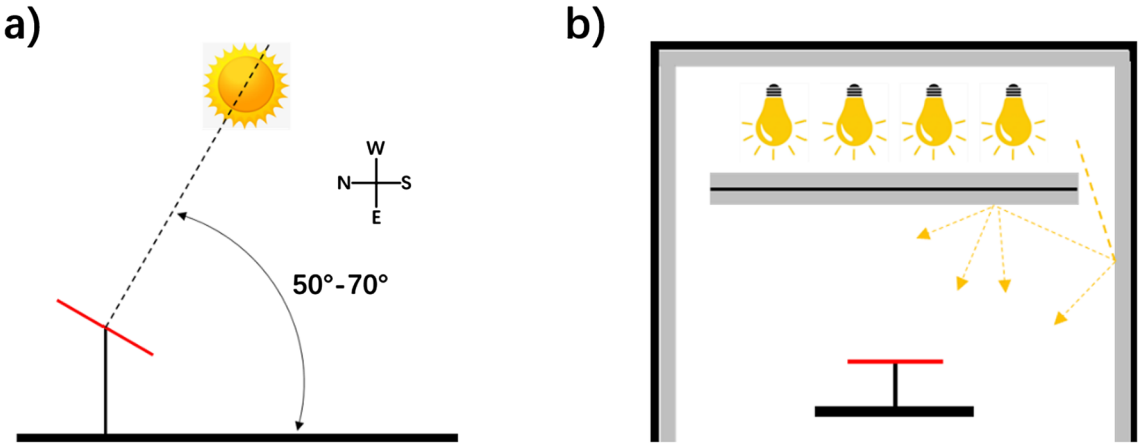

Fig. 3. Schematic representations of an LSC measured under (a) outdoor sunny condition and (b) indoor condition.

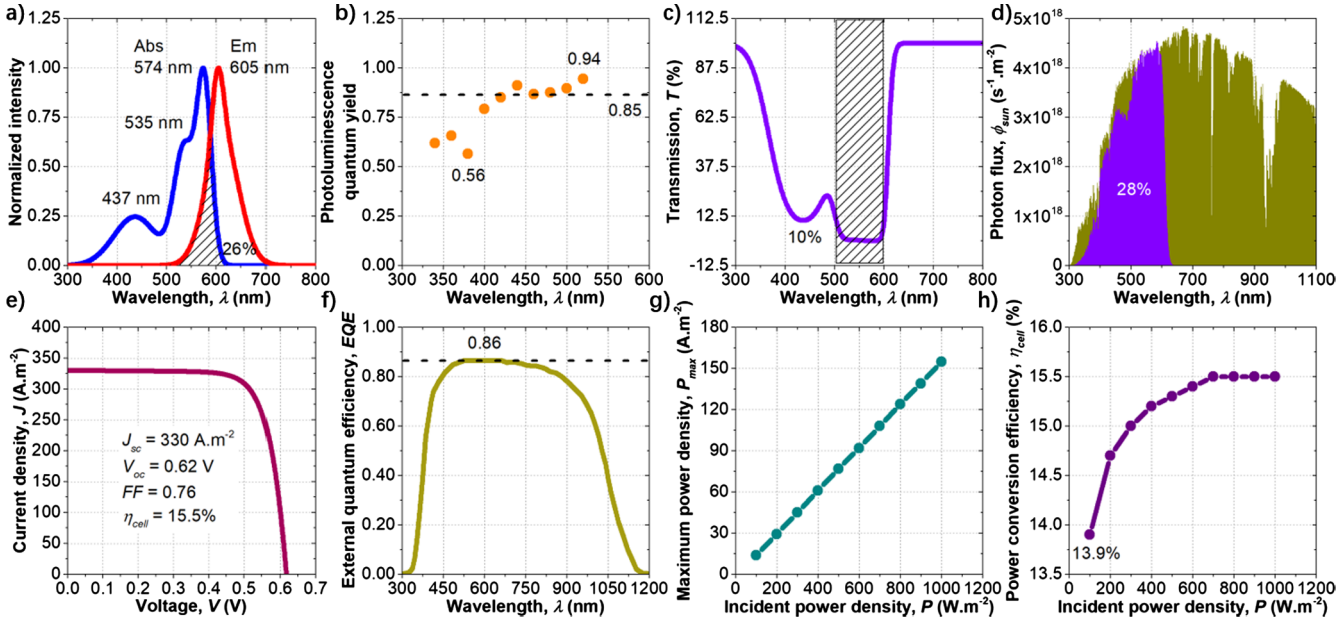

Fig. 4. Spectroscopic properties of R305 in PMMA matrix including (a) absorption and emission spectra and (b) PLQY at different excitation wavelength; (c) transmission spectrum of the luminescent waveguide; (d) percentage of the photons absorbed by the waveguide in the solar spectrum before the band gap of p-Si; (e) *J-V* curve of the solar cells; (f) EQE of the solar cells; (g) relationship between P_{max} and P_{in}; and (h) relationship between η_{cell} and P_{in}.

3.2. Performance of the LSCs under simulated sunlight

We next investigated the performance of the LSCs under AM1.5G simulated sunlight. Attention was paid to J_{sc}, V_{oc}, *FF* and the device power conversion efficiency (η_{LSC}) that were extracted from the *J-V* curves, and their changes with the increase of the waveguide length (L). In addition, the power concentration ratio (C) of the LSCs, which is the power produced from solar cells attaching to the luminescent waveguide relative to the detached status, was measured to show power enhancement of the solar cells by the waveguide. Another parameter, optical collection probability (P), which is the ration between C and the geometric gain (G) of the LSCs (in this study $G = L$), was also measured to show the capability of luminescent waveguide in photon collection and concentration (Desmet et al., 2012). The following equations are shown to clarify the definitions of η_{LSC}; C, P and G and the relationships among these parameters:

$$\eta_{LSC} = \frac{P_{LSC}}{P_{in}} = \frac{P_{LSC}}{H_{in}A_{LSC}} \quad (1)$$

$$C = \frac{P_{LSC}}{P_{cell}} = \frac{P_{LSC}}{P_{in}\eta_{cell}} = \frac{P_{LSC}}{H_{in}A_{cell}\eta_{cell}} \quad (2)$$

$$P = \frac{C}{G} = \frac{\eta_{LSC}}{\eta_{cell}} \quad (3)$$

$$G = \frac{A_{LSC}}{A_{cell}} \quad (4)$$

where P_{LSC} (W) is the electric power produced by the LSC; P_{in} (W) is the incident power on the LSC; H_{in} (W·m^{-2}) is the incident power density; A_{LSC} (m) is the incident area of the LSC, which is the front surface area of the LSC; and A_{cell} is the incident area of the solar cells, which is the edge area of the LSC.

A decrease in J_{sc} was observed (Fig. 5a), suggestive of increasing photon loss possibly due to the self-absorption of the luminophores. In the contrary to J_{sc}, an increase in V_{oc} was observed, implying the increase of the intensity of fluorescent light delivered to the edge-attached solar cells (Fig. 5b). According to the general properties of p-Si solar cells, increasing P_{in} (in this case it was the fluorescent light) also increases the electron-hole recombination rate (Chegaar et al., 2013). This made *FF* show an overall decreasing trend (Fig. 5c). Among the photovoltaic parameters, J_{sc} demonstrated the most apparent change compared to V_{oc} and *FF* and therefore, η_{LSC} was dominated by J_{sc} (Fig. 5d). In terms of the performance of the solar cells, C exhibited almost a linear increase (Fig. 5e). The power produced by the solar cells enhanced by almost 1.5 times in the largest device (L = 12 in.). The decrease trend of P clearly indicated the relationship between the photon collection and photon concentration (Fig. 5f). More photons were collected by the luminescent waveguide because of a larger front surface; however, the photon concentration process became less efficient due to the increase of photon loss, and this photon loss would be significant in large devices. To obtain the performance of the large devices, we applied theoretical methods to project the performance of the LSCs with waveguide length of up to 120 in. (Batchelder et al., 1979, 1981; Currie et al., 2008; Klimov et al., 2016). First, the theoretical results were consistent with the experimental results when L was from 1 in. to 12 in. The projected η_{LSC} exhibited a quasi-exponential decay and were approaching to near 1% when L increased (Fig. 5g) The projected C indicated that the solar cells when attached to the luminescent waveguide with L = 120 in. could produce electricity approximate 8 times higher than they did in detached status (Fig. 5h). And the projected P dropped significantly to below 7% at L = 120 in. (Fig. 5i).

3.3. Performance of the LSCs under outdoor conditions

Our next study was to understand the performance of the LSCs under outdoor conditions. The devices were measured under sunny, overcast and raining conditions and the performance parameters including η_{LSC}, C and P were recorded. These parameters under different outdoor conditions were plotted in the same scale with the increase of L for easy comparison. Under the sunny condition, the devices exhibited a slow decrease in η_{LSC} with the increase of L (Fig. 6a). Compared to those measured under simulated light, η_{LSC} measured under sunny condition were nearly 1.5 times higher. This was possibly due to some characteristics of the outdoor sunlight. The outdoor sunlight contains more photons within the absorption spectrum of the luminophores than the simulated sunlight (Keogh and Blakers, 2004), and it contains indirect component that can be utilized by the LSCs while the simulated light is mostly direct (Press, 1976). Due to the enhancement in η_{LSC}, the power

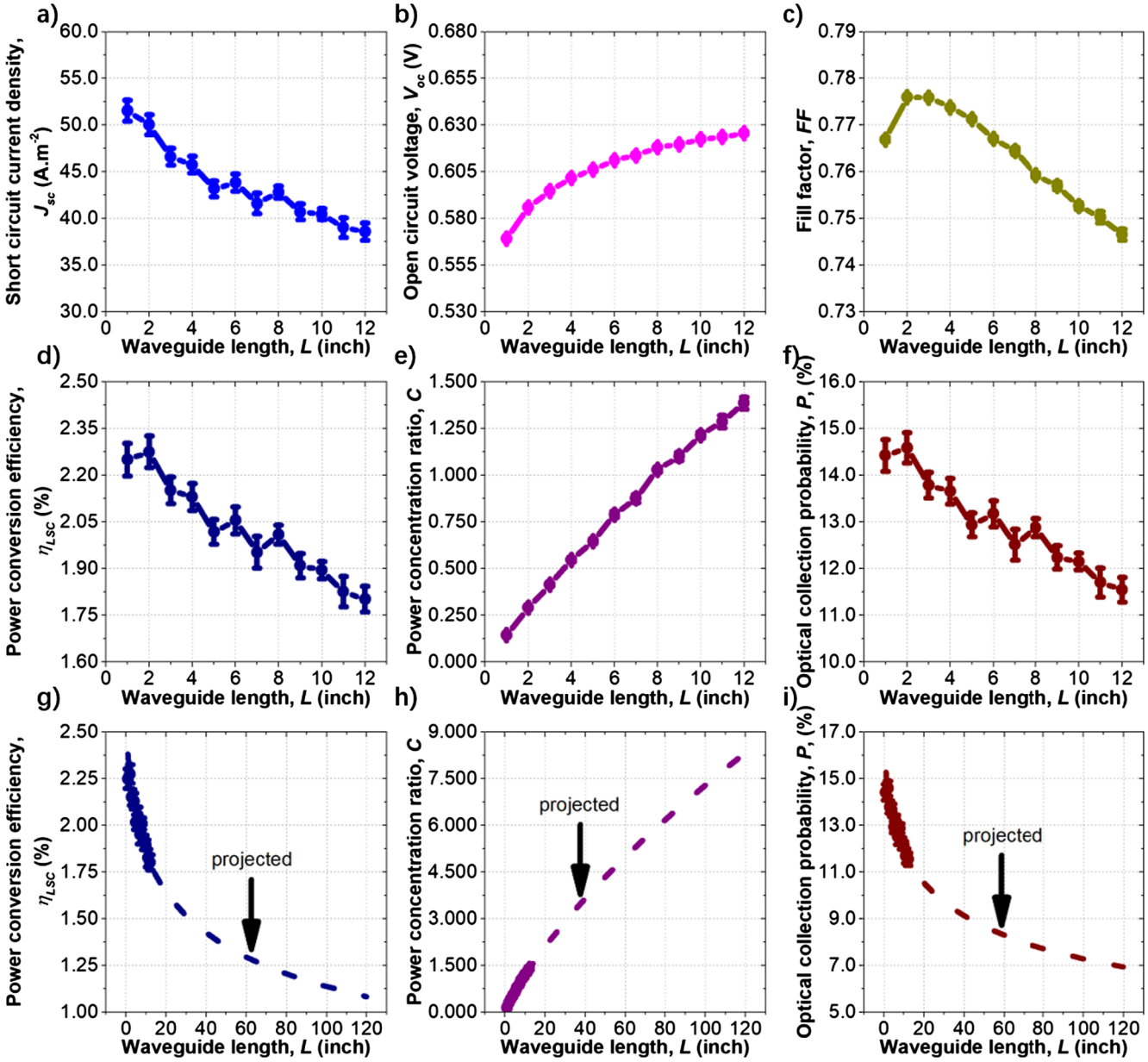

Fig. 5. Photovoltaic parameters and performance of the LSCs including (a) J_{sc}, (b) V_{oc}, (c) *FF*, (d) η_{LSC}, (e) *C* and (f) *P*; and projected (g) η_{LSC}, (h) *C* and (i) *P* of the LSCs at large *L* up to 120 in.

produced from the edge-attached solar cells increased, leading to a *C* of up to 1.9 (Fig. 6b) and *P* of up to 16% (Fig. 6c) at $L = 12$ in., which were much higher than the results measured under the simulated light. Under the overcast condition, a fast decreasing trend was observed for η_{LSC}, in which small devices ($L < 6$ in.) performed much more efficiently than large devices ($L \geq 6$ in.) (Fig. 6d). The significant inefficiency of large devices led to *C* below 1 even at $L = 10$ in. (Fig. 6e), and a fast decay in *P* as well (Fig. 6f). Under the raining condition in which water covered on the front surface of the luminescent waveguide, the device performance further decreased due to the inefficient photon transport by successive TIR affected by the water. Similar trends in η_{LSC} (Fig. 6g), *C* (Fig. 6h) and *P* (Fig. 6i) were observed to those observed under overcast condition. It can see that η_{LSC} measured under overcast and raining conditions was higher than that measured under sunny condition at $L \leq 3$ in. This was possibly because of the indirect light, in which a portion of light was directly absorbed by the solar cells. This phenomenon became more and more ineffective in large devices ($L > 3$ in.) where luminescent light took the majority. The overall difference in the device performance among the sunny, overcast and raining conditions is attributed to the difference in incident spectrum and angle between direct and indirect light (Debije and Rajkumar, 2015). The results of the device performance in the outdoor environment in our study were not completely consistent with a previous report, in which the LSCs were designed as noise barriers for highway application (Kanellis et al., 2017; Debije et al., 2017a, 2017b). The inconsistency suggested that the actual performance of the LSCs in the outdoor environment highly depended on the configuration of the device (*e.g.*, luminophores and solar cells) and condition of measurement (*e.g.*, location and temperature).

3.4. Performance of the LSCs under indoor conditions

Our final study was to investigate the performance of the LSCs under indoor conditions. Four different types of common indoor light bulbs were used. They were incandescent, halogen, fluorescent and light-emitting diode (LED). Before the measurement, the emission

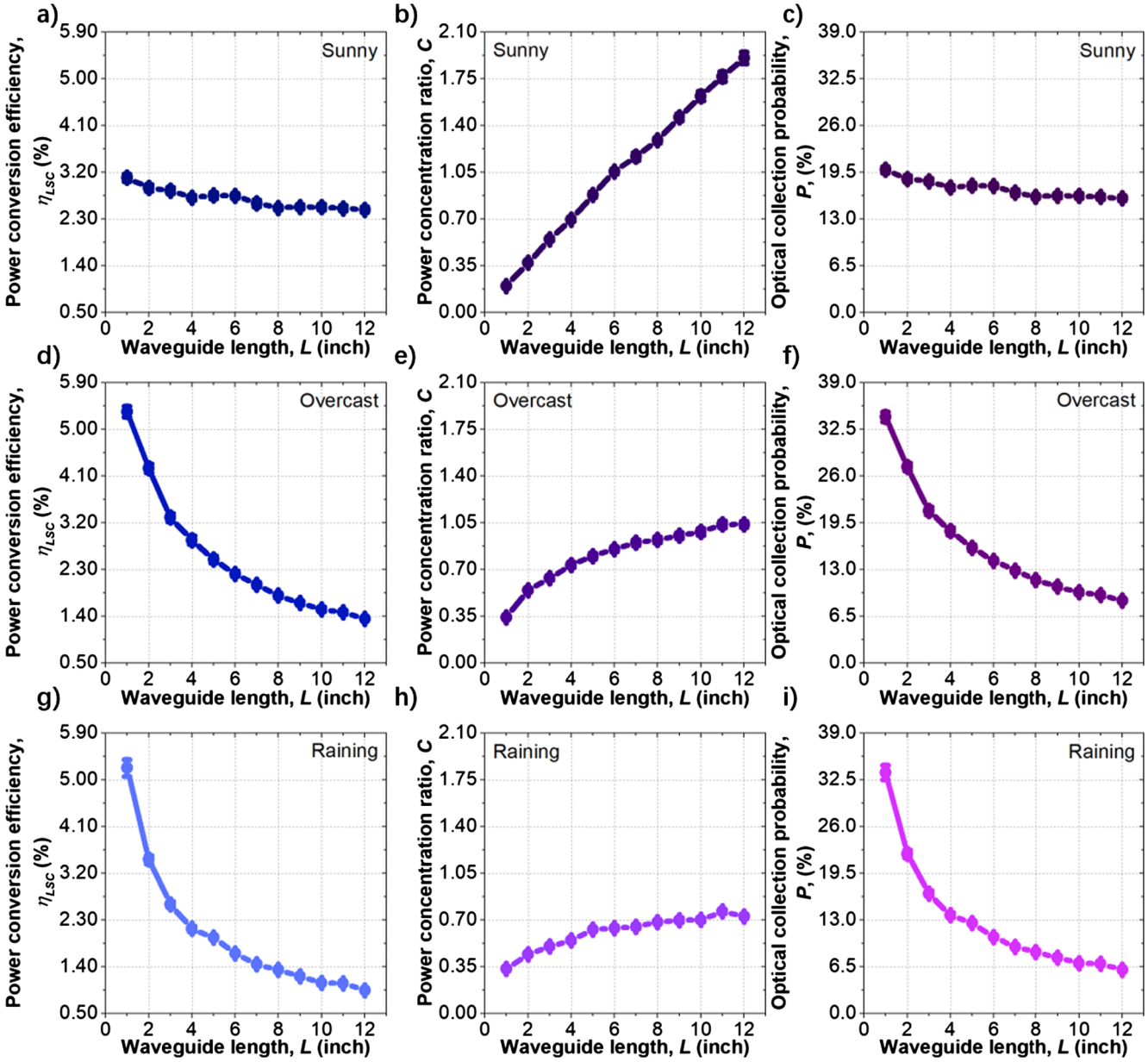

Fig. 6. The performance of the LSCs including (a) η_{LSC}, (b) C and (c) P measured under outdoor sunny condition; (d) η_{LSC}, (e) C and (f) P measured under outdoor overcast condition; and (g) η_{LSC}, (h) C and (i) P measured under outdoor raining condition.

spectra of the four indoor light bulbs were measured. In the incandescent condition, orange-red light was the majority in the spectrum (Fig. 7a), and the spectrum of halogen condition was similar to that of the incandescent condition (Fig. 7b). The fluorescent condition showed scattered spectrum where the primary peaks were around 450 nm, 550 nm and 600 nm (Fig. 7c). In the LED condition, the spectrum showed a maximum at 600 nm and a second maximum at 450 nm (Fig. 7d). In the measurement, only η_{LSC} were recorded. The C and P of the LSCs were not measured because the performance of solar cells under indoor conditions couldn't be measured due to very low P_{in}. Same to the outdoor conditions, η_{LSC} exhibited an increasing trend with the increase of L. The η_{LSC} measured under the incandescent condition was very low below 0.25% (Fig. 7e), while much improved η_{LSC} by approximate 1.1% were obtained under the halogen condition (Fig. 7f). Surprisingly, very high η_{LSC} were obtained in the fluorescent condition (Fig. 7g) and LED condition (Fig. 7h). The difference in η_{LSC} under different indoor conditions were attributed to the number of photons within the absorption range of the luminophores relative to the number of photons in the light spectrum, which were 13%, 22%, 60% and 49% for incandescent, halogen, fluorescent and LED conditions, respectively (Fig. 7a–d).

4. Conclusions and remark

In summary, we investigated the performance of the LSCs with different sizes under different light conditions. The performance of the LSCs were measured outdoor conditions included sunny (direct, $1000\ W{\cdot}m^{-2} \pm 100\ W{\cdot}m^{-2}$), overcast (indirect, $100\ W{\cdot}m^{-2} \pm 10\ W{\cdot}m^{-2}$) and raining (indirect, $50\ W{\cdot}m^{-2} \pm 5\ W{\cdot}m^{-2}$) conditions. The LSCs exhibited higher power conversion efficiency (η_{LSC}) and power concentration ratio (C) under outdoor sunny condition (η_{LSC} = 3.09–2.48% and C = 0.20–1.91) than under simulated sunlight (η_{LSC} = 2.28–1.80% and C = 0.14–1.39). The η_{LSC} of the LSCs decreased rapidly with the increase of the device size (L = 1–12 in.) under overcast (η_{LSC} = 5.34–1.35%) and raining (η_{LSC} = 5.22–0.94%) conditions. This was due to inefficiency of the luminescent waveguide in photon collection

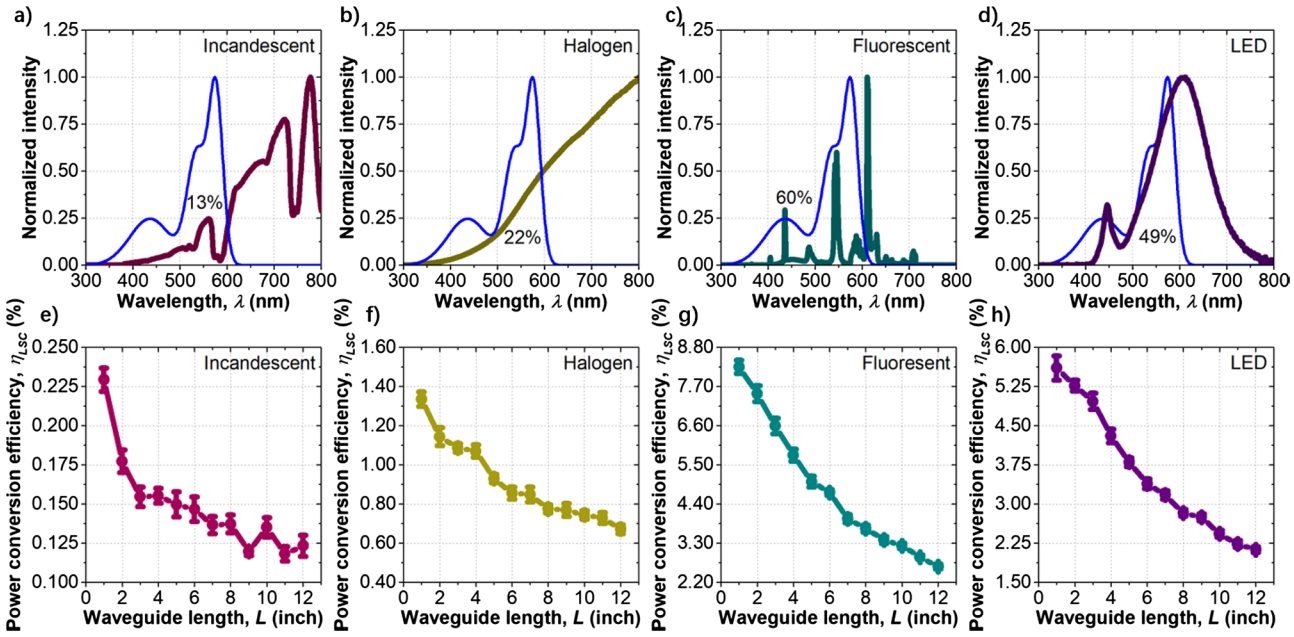

Fig. 7. The spectra of (a) incandescent, (b) halogen, (c) fluorescent and (d) LED light (absorption spectrum of R305 was superimposed and the corresponding percentages of the photons within the absorption was indicated); and η_{LSC} measured under (e) incandescent, (f) halogen, (g) fluorescent and (h) LED conditions.

and concentration (P from over 30% to below 10%). Under indoor conditions (indirect, 10 $W{\cdot}m^{-2}$ ± 1 $W{\cdot}m^{-2}$), the LSCs exhibited much higher η_{LSC} under fluorescent (η_{LSC} = 8.25–2.64%) and LED light (η_{LSC} = 5.60–2.13%) than under incandescent (η_{LSC} = 0.23–0.12%) and halogen light (η_{LSC} = 1.34–0.67%).

The results suggested more promising application of the LSCs in the indoor environment than in the outdoor environment. Unlike the outdoor environment where the light condition is changeable due to weather (*i.e.*, sunny, overcast and raining), the indoor environment typically offers a stable light condition, which is beneficial to the operation and maintenance of the LSCs. Moreover, nowadays most indoor environment is lightened by energy-saving fluorescent and LED light bulbs. The high percentage of visible spectrum in these light conditions improves the performance of the LSCs, as evidenced in our study using R305 (Fig. 7g and h). It is reasonable to believe that the use of other luminophores with other colors (*e.g.*, Lumogen F series: V570, Y083 and O240) also leads to improved device performance in indoor environment compared to the outdoor environment. It should be noted that the indoor application of the LSCs should be different from the outdoor application in the installation scale and the consideration of comfort. In the outdoor application such as building windows and facades that require large-area installation, the LSCs obviously modify the appearance of the luminous environment offered by the building and can affect people's visual comfort (Fig. 1b). For example, a luminous facade made of colorful LSCs will not be suitable for a building in a central business area because this does not match people's understanding on business activities, which should be formal and serious. Also, people will not feel comfortable when living in a luminous area surrounded by colorful LSCs. A previous study on visual performance of a red LSC windows in an office environment suggested no more than 25% coverage of the entire window area for interior views (Vossen et al., 2016). In most cases, people prefer an indoor area with warm white light or daylight. In the indoor application, it is not necessary to install the LSCs in a large scale because the indoor light energy is not a major renewable source due to a relatively lower light intensity compared to the outdoor light. The LSCs in the indoor environment should be applied as accessories in the indoor design and decoration, which play the role of indoor light energy recycling and serve as a minor renewable energy source for buildings. For example, they can be designed as office space dividers, folding partitions and display walls (Fig. 1c). They can be designed with sense of art and aesthetics and placed in living and common areas where additional visual comfort is required.

Acknowledgement

The authors would like to thank Solera City Energy for financial support and the open-access research facilities at Rice University, University of Washington and University of Houston for instrumentation.

References

Akwa, J.V., et al., 2014. Evaluation of the photovoltaic generation potential and real-time analysis of the photovoltaic panel operation on a building facade in southern Brazil. Energy Build. 69, 426–433. https://doi.org/10.1016/j.enbuild.2013.11.007.

Batchelder, J.S., et al., 1979. Luminescent solar concentrators. 1: theory of operation and techniques for performance evaluation. Appl. Opt. 18 (18), 3090–3110. https://doi.org/10.1364/ao.18.003090.

Batchelder, J.S., et al., 1981. Luminescent solar concentrators. 2: experimental and theoretical analysis of their possible efficiencies. Appl. Opt. 20 (21), 3733–3754. https://doi.org/10.1364/ao.20.003733.

Bergren, M.R., et al., 2018. High-performance $CuInS_2$ quantum dot laminated glass luminescent solar concentrators for windows. ACS Energy Lett. 3 (3), 520–525. https://doi.org/10.1021/acsenergylett.7b01346.

Chandra, S., et al., 2012. Enhanced quantum dot emission for luminescent solar concentrators using plasmonic interaction. Sol. Energy Mater. Sol. Cells 98, 385–390. https://doi.org/10.1016/j.solmat.2011.11.030.

Chegaar, M., et al., 2013. Effect of illumination intensity on solar cells parameters. Energy Procedia 36, 722–729. https://doi.org/10.1016/j.egypro.2013.07.084.

Chen, W., et al., 2017. Heavy metal free nanocrystals with near infrared emission applying in luminescent solar concentrator. Solar RRL 1 (6), 1700041. https://doi.org/10.1002/solr.201700041.

Connell, R., et al., 2018. Designing spectrally-selective mirrors for use in luminescent solar concentrators. J. Opt. 20 (2), 024009. https://doi.org/10.1088/2040-8986/aaa074.

Connell, R., Ferry, V.E., 2016. Integrating photonics with luminescent solar concentrators: optical transport in the presence of photonic mirrors. J. Phys. Chem. C 120 (37), 20991–20997. https://doi.org/10.1021/acs.jpcc.6b03304.

Currie, M.J., et al., 2008. High-efficiency organic solar concentrators for photovoltaics. Science 321 (5886), 226–228. https://doi.org/10.1126/science.1158342.

Damrongsak, P., Locharoenrat, K., 2017. Optical performance of fluorescent collectors integrated with microlens arrays. Mater. Res. Express 4 (9), 095502. https://doi.org/10.1088/2053-1591/aa8a1b.

Debije, M.G., et al., 2010. Effect on the output of a luminescent solar concentrator on application of organic wavelength-selective mirrors. Appl. Opt. 49 (4), 745–751. https://doi.org/10.1364/ao.49.000745.

Debije, M.G., et al., 2017a. The solar noise barrier project: 2. The effect of street art on performance of a large scale luminescent solar concentrator prototype. Renew.

Energy 113, 1288–1292. https://doi.org/10.1016/j.renene.2017.07.025.
Debije, M.G., et al., 2017b. The solar noise barrier project: 3. The effects of seasonal spectral variation, cloud cover and heat distribution on the performance of full-scale luminescent solar concentrator panels. Renew. Energy 116A, 335–343. https://doi.org/10.1016/j.renene.2017.09.079.
Debije, M.G., Rajkumar, V.A., 2015. Direct versus indirect illumination of a prototype luminescent solar concentrator. Sol. Energy 122, 334–340. https://doi.org/10.1016/j.solener.2015.08.036.
Debije, M.G., Verbunt, P.P.C., 2012. Thirty years of luminescent solar concentrator research: solar energy for the built environment. Adv. Energy. Mater. 2 (1), 12–35. https://doi.org/10.1002/aenm.201100554.
Desmet, L., et al., 2012. Monocrystalline silicon photovoltaic luminescent solar concentrator with 4.2% power conversion efficiency. Opt. Lett. 37 (15), 3087–3089. https://doi.org/10.1364/ol.37.003087.
Fahad, M., et al., 2017. Metal nanoparticles based stack structured plasmonic luminescent solar concentrator. Sol. Energy 155, 934–941. https://doi.org/10.1016/j.solener.2017.07.037.
Freitas, V.T., et al., 2015. Eu^{3+}-based bridged silsesquioxanes for transparent luminescent solar concentrators. ACS Appl. Mater. Interfaces 7 (16), 8770–8778. https://doi.org/10.1021/acsami.5b01281.
Frias, A.R., et al., 2019. Transparent luminescent solar concentrators using Ln^{3+}-based ionosilicas towards photovoltaic windows. Energies 12 (3), 451. https://doi.org/10.3390/en12030451.
Goetzberger, A., Greube, W., 1977. Solar energy conversion with fluorescent collectors. Appl. Phys. 14 (2), 123–139. https://doi.org/10.1007/bf00883080.
Griffini, G., et al., 2013. Novel crosslinked host matrices based on fluorinated polymers for long-term durability in thin-film luminescent solar concentrators. Sol. Energy Mater. Sol. Cells 118, 36–42. https://doi.org/10.1016/j.solmat.2013.05.041.
Iasilli, G., et al., 2019. Luminescent solar concentrators: boosted optical efficiency by polymer dielectric mirrors. Mater. Chem. Front. 3 (3), 429–436. https://doi.org/10.1039/c8qm00595h.
Kanellis, M., et al., 2017. The solar noise barrier project: 1. Effect of incident light orientation on the performance of a large-scale luminescent solar concentrator noise barrier. Renew. Energy 103, 647–652. https://doi.org/10.1016/j.renene.2016.10.078.
Kang, H., et al., 2019. Techno-economic performance analysis of the smart solar photovoltaic blinds considering the photovoltaic panel type and the solar tracking method. Energy Build. 193, 1–14. https://doi.org/10.1016/j.enbuild.2019.03.042.
Keogh, W.M., Blakers, A.W., 2004. Accurate measurement, using natural sunlight, of silicon solar cells. Prog. Photovoltaics 12 (1), 1–19. https://doi.org/10.1002/pip.517.
Kerrouche, A., et al., 2014. Luminescent solar concentrators: from experimental validation of 3D ray-tracing simulations to coloured stained-glass windows for BIPV. Sol. Energy Mater. Sol. Cells 122, 99–106. https://doi.org/10.1016/j.solmat.2013.11.026.
Klimov, V.I., et al., 2016. Quality factor of luminescent solar concentrators and practical concentration limits attainable with semiconductor quantum dots. ACS Photon. 3 (6), 1138–1148. https://doi.org/10.1021/acsphotonics.6b00307.
Knowles, K.E., et al., 2015. Bright $CuInS_2$/CdS nanocrystal phosphors for high-gain full-spectrum luminescent solar concentrators. Chem. Commun. 51 (44), 9129–9132. https://doi.org/10.1039/c5cc02007g.
Krumer, Z., et al., 2013. Tackling self-absorption in luminescent solar concentrators with type-II colloidal quantum dots. Sol. Energy Mater. Sol. Cells 111, 57–65. https://doi.org/10.1016/j.solmat.2012.12.028.
Kurmi, I., et al., 2018. Micro-lens aperture array for enhanced thin-film imaging using luminescent concentrators. Opt. Express 26 (2), 29253–29261. https://doi.org/10.1364/oe.26.029253.
Lai, C.-M., Hokoi, S., 2015. Solar façades: a review. Build. Environ. 91, 152–165. https://doi.org/10.1016/j.buildenv.2015.01.007.
Li, Y., et al., 2012. Synthesis and characterizations of benzothiadiazole-based fluorophores as potential wavelength-shifting materials. J. Photochem. Photobiol. A 231 (1), 51–59. https://doi.org/10.1016/j.jphotochem.2012.01.011.
Li, Y., et al., 2013. Tuning photophysical properties of triphenylamine and aromatic cyano conjugate-based wavelength-shifting compounds by manipulating intramolecular charge transfer strength. J. Photochem. Photobiol. A 251, 1–9. https://doi.org/10.1016/j.jphotochem.2012.10.002.
Li, Y., et al., 2015. Enhancing the output current of a CdTe solar cell via a CN-free hydrocarbon luminescent down-shifting fluorophore with intramolecular energy transfer and restricted internal rotation characteristics. Photochem. Photobiol. Sci. 14 (4), 833–841. https://doi.org/10.1039/c4 pp00480a.
Li, Y., et al., 2016. A structurally modified perylene dye for efficient luminescent solar concentrators. Sol. Energy 136, 668–674. https://doi.org/10.1016/j.solener.2016.07.051.
Li, Y., et al., 2019. Review on the role of polymers in luminescent solar concentrators. J. Polym. Sci. A 57 (3), 201–215. https://doi.org/10.1002/pola.29192.
Li, Y., Liu, C., 2018. Techno-economic analysis for constructing solar photovoltaic projects on building envelopes. Build. Environ. 127, 37–46. https://doi.org/10.1016/j.buildenv.2017.10.014.
Liu, C., et al., 2014. Luminescent solar concentrators fabricated by dispersing rare earth particles in PMMA waveguide. Int. J. Photoenergy 2014, 290952. https://doi.org/10.1155/2014/290952.
Meinardi, F., et al., 2015. Highly efficient large-area colourless luminescent solar concentrators using heavy-metal-free colloidal quantum dots. Nat. Nanotechnol. 10, 878–885. https://doi.org/10.1038/nnano.2015.178.
Meinardi, F., et al., 2017. Doped halide perovskite nanocrystals for reabsorption-free luminescent solar concentrators. ACS Energy Lett. 2 (10), 2368–2377. https://doi.org/10.1021/acsenergylett.7b00701.
Moraitis, P., et al., 2018. Nanoparticles for luminescent solar concentrators – a review. Opt. Mater. 84, 636–645. https://doi.org/10.1016/j.optmat.2018.07.034.
Mouedden, Y.E., et al., 2015. A cost-effective, long-lifetime efficient organic luminescent solar concentrator. J. Appl. Phys. 118, 015502. https://doi.org/10.1063/1.4923389.
Powell, D., et al., 2018. A reflective adaptive solar façade for multi-building energy and comfort management. Energy Build. 177, 303–315. https://doi.org/10.1016/j.enbuild.2018.07.040.
Press, W.H., 1976. Theoretical maximum for energy from direct and diffuse sunlight. Nature 264, 734–735. https://doi.org/10.1038/264734a0.
Purcell-Milton, F., Gun'ko, Y.K., 2012. Quantum dots for luminescent solar concentrators. J. Mater. Chem. 22 (33), 16687–16697. https://doi.org/10.1039/c2jm32366d.
Reinders, A., et al., 2018. Luminescent solar concentrator photovoltaic designs. Jpn. J. Appl. Phys. 57 (8S3), 08RD10. https://doi.org/10.7567/JJAP.57.08RD10.
Sala, P.D., et al., 2019. First demonstration of the use of very large Stokes shift cycloparaphenylenes as promising organic luminophores for transparent luminescent solar concentrators. Chem. Commun. 55 (21), 3160–3163. https://doi.org/10.1039/c8cc09859j.
Sanguineti, A., et al., 2012. NIR emitting ytterbium chelates for colourless luminescent solar concentrators. Phys. Chem. Chem. Phys. 14 (18), 6452–6455. https://doi.org/10.1039/c2cp40791d.
Sanguineti, A., et al., 2013. High Stokes shift perylene dyes for luminescent solar concentrators. Chem. Commun. 49 (16), 1618–1620. https://doi.org/10.1039/c2cc38708e.
Shcherbatyuk, G.V., et al., 2010. Viability of using near infrared PbS quantum dots as active materials in luminescent solar concentrators. Appl. Phys. Lett. 96 (19), 191901. https://doi.org/10.1063/1.3422485.
Slooff, L.H., et al., 2008. A luminescent solar concentrator with 7.1% power conversion efficiency. Phys. Status Solidi RRL 2 (6), 257–259. https://doi.org/10.1002/pssr.200802186.
ten Kate, O., et al., 2015. Efficient luminescent solar concentrators based on self-absorption free, Tm2+ doped halides. Sol. Energy Mater. Sol. Cells 140, 115–120. https://doi.org/10.1016/j.solmat.2015.04.002.
Tseng, J.K., et al., 2011. Application of optical film with micro-lens array on a solar concentrator. Sol. Energy 85 (9), 2167–2178. https://doi.org/10.1016/j.solener.2011.06.004.
Tsoi, S., et al., 2013. Using lenses to improve the output of a patterned luminescent solar concentrator. Adv. Energy. Mater. 3 (3), 337–341. https://doi.org/10.1002/aenm.201200395.
Tummeltshammer, C., et al., 2013. Efficiency and loss mechanisms of plasmonic luminescent solar concentrators. Opt. Express 21 (S5), A735–A749. https://doi.org/10.1364/oe.21.00a735.
van Sark, W., et al., 2008. Luminescent solar concentrators - a review of recent results. Opt. Express 16 (26), 21773–21792. https://doi.org/10.1364/oe.16.021773.
van Sark, W., et al., 2017. The “electric mondrian” as a luminescent solar concentrator demonstrator case study. Solar RRL 1 (3–4), 1600015. https://doi.org/10.1002/solr.201600015.
Verbunt, P.P., et al., 2012. Increased efficiency of luminescent solar concentrators after application of organic wavelength selective mirrors. Opt. Express 20 (S5), A655–A668. https://doi.org/10.1364/oe.20.00a655.
Vossen, F.M., et al., 2016. Visual performance of red luminescent solar concentrating windows in an office environment. Energy Build. 113, 123–132. https://doi.org/10.1016/j.enbuild.2015.12.022.
Wang, T., et al., 2011. Luminescent solar concentrator employing rare earth complex with zero self-absorption loss. Sol. Energy 85 (11), 2571–2579. https://doi.org/10.1016/j.solener.2011.07.014.
Weber, W.H., Lambe, J., 1976. Luminescent greenhouse collector for solar radiation. Appl. Opt. 15 (10), 2299–2300. https://doi.org/10.1364/ao.15.002299.
Wilson, L.R., et al., 2010. Characterization and reduction of reabsorption losses in luminescent solar concentrators. Appl. Opt. 49 (9), 1651–1661. https://doi.org/10.1364/ao.49.001651.
Xu, L., et al., 2016. Enhanced photon collection in luminescent solar concentrators with distributed Bragg reflectors. ACS Photon. 3 (2), 278–285. https://doi.org/10.1021/acsphotonics.5b00630.
Yang, C., et al., 2018. Impact of stokes shift on the performance of near-infrared harvesting transparent luminescent solar concentrators. Sci. Rep. 8 (1), 16359. https://doi.org/10.1038/s41598-018-34442-3.
Yang, C., et al., 2019. Integration of near-infrared harvesting transparent luminescent solar concentrators onto arbitrary surfaces. J. Luminesc. 210, 239–246. https://doi.org/10.1016/j.jlumin.2019.02.042.
Zalewski, L., et al., 2002. Study of solar walls - validating a simulation model. Build. Environ. 37 (1), 109–121. https://doi.org/10.1016/S0360-1323(00)00072-X.
Zhang, B., et al., 2018. Aggregation-induced emission-mediated spectral downconversion in luminescent solar concentrators. Mater. Chem. Front. 2 (3), 615–619. https://doi.org/10.1039/c7qm00598a.
Zhao, Y., et al., 2014. Near-Infrared harvesting transparent luminescent solar concentrators. Adv. Opt. Mater. 2 (7), 606–611. https://doi.org/10.1002/adom.201400103.
Zhao, Y., Lunt, R.R., 2013. Transparent luminescent solar concentrators for large-area solar windows enabled by massive Stokes-shift nanocluster phosphors. Adv. Energy. Mater. 3 (9), 1143–1148. https://doi.org/10.1002/aenm.201300173.
Zhou, Y., et al., 2016. Near infrared, highly efficient luminescent solar concentrators. Adv. Energy Mater. 6 (11), 1501913. https://doi.org/10.1002/aenm.201501913.
Zhou, Y., et al., 2018. Harnessing the properties of colloidal quantum dots in luminescent solar concentrators. Chem. Soc. Rev. 47 (15), 5866–5890. https://doi.org/10.1039/c7cs00701a.